Global Biogeochemical Cycles

Supporting Information for

Flux of particulate elements in the North Atlantic Ocean constrained by multiple radionuclides

Christopher T. Hayes[1], Erin E. Black[2], Robert F. Anderson[3,4], Mark Baskaran[5], Ken O. Buesseler[2], Matthew A. Charette[2], Hai Cheng[6,7], J. Kirk Cochran[8], R. Lawrence Edwards[7], Patrick Fitzgerald[8], Phoebe J. Lam[9], Yanbin Lu[10], Stephanie O. Morris, Daniel C. Ohnemus[11], Frank J. Pavia[3,4], Gillian Stewart[12,13], Yi Tang[12,13] (alphabetical after first 2 authors)

Contents of the Supporting information

[1] School of Ocean Science and Technology, University of Southern Mississippi, Stennis Space Center, MS, USA
[2] Woods Hole Oceanographic Institution, Woods Hole, MA, USA
[3] Department of Earth and Environmental Sciences, Columbia University, New York, NY, USA
[4] Lamont-Doherty Earth Observatory of Columbia University, Palisades, NY, USA
[5] Department of Geology, Wayne State University, Detroit, MI, USA
[6] Institute of Global Environmental Change, Xi'an Jiaotong University, Xi'an, China
[7] Department of Earth Sciences, University of Minnesota, Minneapolis, MN USA
[8] School of Marine and Atmospheric Science, Stony Brook University, Stony Brook, NY USA
[9] Ocean Sciences Department, University of California Santa Cruz, Santa Cruz, CA USA
[10] Earth Observatory of Singapore, Nanyang Technical University, Singapore
[11] Bigelow Laboratory for Ocean Sciences, East Boothbay, ME USA
[12] School of Earth and Environmental Sciences, City University of New York, Flushing, NY USA
[13] Earth and Environmental Sciences Program, The Graduate Center, City University of New York, New York, NY USA

Supplemental Text 1.

Total and Particulate ^{234}Th in Water Samples from the Bermuda Rise Flux Experiment (BaRFlux)

Methods

Cruise Information

The Bermuda Rise (33°N, 55°W), is a sediment drift accumulation site near the Bermuda Ocean Time Series (BATS) sampling station. It is a relative bathymetric high and has an uncharacteristically high sedimentation rate for an oligotrophic open-ocean gyre environment. Six cruises were conducted to the Bermuda Rise between November of 2011 and June of 2013, using both the R/V *Endeavor* and the R/V *Atlantic Explorer*.

Sample Collection

Filterable Particles

Particles were collected by Challenger *in situ* pumps for ^{234}Th and organic carbon measurement, filtering roughly one cubic meter of seawater over the course of two hours. Samples were taken at a range of depths spanning the water column to create a profile from the euphotic zone to the seasonal benthic nepheloid layer. Sequential 142-mm filters were used to sort particles by size fraction. Large particles were collected on polyester (Petex) filters with a nominal pore size of 70 µm. Smaller particles were collected on quartz microfiber filters (Whatman QM-A) with a nominal pore size of 1 µm. Additionally, on the June 2013 cruise only, some filtrations were conducted using polyethersulfone membrane (Supor) filters with a nominal pore size of 0.8 µm, instead of Whatman QM-A. These filtrations were done by pairing pumps 20 m apart (Table S1), with one pump using 70-µm polyester filters and QM-A and the other using 70-µm polyester filters with Supor. Furthermore, on the final two cruises of the project, quartz microfiber filters were doubled up, for a total of 3 filters in each pump (Polyester filter / top QM-A / bottom QM-A), in order to test sorption of dissolved ^{234}Th onto the QM-A filters or bleed-through of particles from the upper QM-A.

After retrieval of the pumps, filters were removed and water volumes as well as pumping times were recorded. Polyester filters were divided in halves for radiochemical and organic geochemical analyses. Thorium fractions were rinsed off of the filter onto a 2.5-cm quartz microfiber filter, dried for 24 hours at 30°C, and then mounted for eventual beta counting. Organic carbon fractions were also rinsed onto quartz filters, and frozen.

Then 142 mm Quartz microfiber filters were likewise divided in halves for radiochemical and organic geochemical analyses. Thorium fractions were dried for 24 hours at 30°C. Ten 2.5-cm discs were punched out of each quartz filter, stacked together, and mounted for beta counting. Fractions for organic carbon analysis were promptly frozen when recovered. On cruises in which these filters were double-layered, no portion of the back layer went to organic carbon analysis.

Polyethersulfone membrane (Supor) filters were used only for radiochemical analysis. Filters were dried for 24 hours at 30°C. Due to the thinner size of this filter, more discs were required to fill the beta counting cups. Twenty 2.5-cm discs were punched out of each dried membrane filter and stacked together for beta counting.

Water samples

Unfiltered seawater was obtained for ^{234}Th measurement by 10-L Niskin bottles attached to a CTD rosette throughout the upper 300 m of the water column, to create a profile of the zone of maximum biological activity. Water for ^{234}Th measurement was then transferred to 2.5-L polycarbonate bottles and acidified to pH 2 with 6N hydrochloric acid for storage.

In the laboratory, water samples were further processed within two weeks of collection. A ^{230}Th tracer was added to each sample. Manganese oxide precipitation was carried out by adding manganese chloride and potassium permanganate before adjusting the pH to ~8 with concentrated ammonium hydroxide. The resulting precipitate, containing the Th, was collected by vacuum filtration onto 2.5-cm quartz microfiber filters, which were then dried and mounted for beta counting.

Analysis

^{234}Th determination

Activities of ^{234}Th were measured by counting beta emissions via published methodolodies (Buesseler et al., 2001; Cochran and Masqué, 2003). Samples were counted four times, with the first count happening within a month of sample collection, and the final count occurring roughly six months after collection, when any excess ^{234}Th activity in the sample had decayed away. The excess activity was determined by plotting the activity at each interval against $[1 - e^{-\lambda t}]$, where λ is the decay constant of ^{234}Th and t is the amount of time between collection and counting. The excess ^{234}Th activity at the time of initial counting was given by the slope of the plot (note that all particulate ^{234}Th activities reported in this document are excess activities). Activities were then corrected to the time of sample collection, accounting for any ingrowth of ^{234}Th between collection and precipitation of MnO_2. ^{238}U activities were estimated from the established relationship between U and salinity (Pates and Muir, 2007).

Recovery of ^{234}Th from the water samples was determined by measuring the ^{230}Th tracer after beta emissions counting was complete. Samples were dissolved by heating the filters gently in 10 mL of nitric acid with 1 mL of hydrofluoric acid until no solid particles remained. Then thorium was isolated and purified on anion exchange resin (Bio-Rad AG 1-X8) as described in (Auro et al., 2012). Finally, ^{230}Th was measured by inductively coupled plasma mass spectrometry (ICP-MS) using either a Thermo Element 2 or Nu Plasma 2 mass spectrometer.

Filter punches for carbon analysis were taken from the organic geochemical splits of the filters. For particulate organic carbon (POC) measurement, the filter punches were gently acidified to remove calcium carbonate. Carbon was then measured on a CNS analyzer as previously described (Abramson et al., 2010).

Results and Discussion

Filterable Particles

Particulate ^{234}Th

Particulate ^{234}Th is primarily distributed in the small (1-70 µm) size fraction, while a smaller amount of ^{234}Th activity is found in the large (>70 µm) fraction (Figure S1; Dataset S1

Table S2). This finding is consistent with our understanding that thorium sorbs to surfaces relatively unselectively, and thus is fractionated between particle classes according to the total available surface area associated with each class.

Particulate ^{234}Th activity in both size classes is highest near the surface, reflecting a high amount of particle surface area due to biological productivity (Fig. S1). At many times of the year there is also a local maximum in particulate ^{234}Th activity near the bottom of the water column, due to particles suspended in the seasonal nepheloid layer. The effect of the nepheloid layer is measurable in both size classes, but appears to be more pronounced in smaller particles.

When water was filtered at the same depth one or more days apart (as in May 2012; Table S2), temporal variability in particulate ^{234}Th activity was greatest near the surface of the water, and diminished with depth. Since this effect was greatest in the euphotic zone, it was likely caused by diurnal cycles in biological activity.

On the June 2013 cruise, different modes of filtration were employed. When two QM-A filters were stacked together beneath the polyester filter, ^{234}Th activity was detected on both filters, with a smaller, but non-trivial, activity on the lower filter (QMA-2) (Table S1). Two proposed mechanisms for ^{234}Th to reach the second QM-A filter are bleed-through of particles from the first filter, and sorption of dissolved thorium. Activity on the second filter was greatest at water depths where particulate activity was highest (in the euphotic zone and in the seasonal nepheloid layer), rather than at mid-water depths where dissolved ^{234}Th is most abundant (Table S1). Thus the bleed-through of particles from the first filter to the second seems to be the dominant mechanism by which ^{234}Th arrives on the second QM-A filter.

Also on the June 2013 cruise, 0.8-µm Supor filters were deployed for comparison with QM-A filters. The activity of particulate ^{234}Th retained on these filters was similar to that of QM-A filters, to the extent that differences between the two filters can be distinguished from spatiotemporal variation in the water column. Knowing that both filters produce similar results for ^{234}Th is important because the type of filter used may need to be chosen to fulfill other analytical needs such as measurement of organic carbon or longer-lived metal isotopes.

Particulate organic carbon

POC was most abundant near the surface and generally declined with depth. Unlike thorium, there was no local maximum of POC in the benthic nepheloid layer. POC was much more abundant in the small size fraction than in the large size fraction (Dataset S1**Error! Reference source not found.**). POC in the euphotic zone is strongly seasonal, with much greater concentrations found in May and June than during other cruises.

Also during May and June, the POC-to-^{234}Th ratios (POC/^{234}Th) found were greater in the small size fraction, whereas measurements during other months showed elevated POC/^{234}Th in the large size fraction (Fig. S1). In biogenic particles, organic carbon is expected to scale with the volume of particles, but ^{234}Th is expected to scale with the surface area of particles, because carbon is inside the particles and thorium is sorbed to their exteriors. Accordingly, one would normally expect a higher POC/^{234}Th in larger particles, which have a high volume/area ratio. This is consistent with our findings that large particles have a higher POC/^{234}Th at the Bermuda Rise (where lithogenic particles are scarce in the upper water column) for most of the year. However, in May, 2012 and June, 2013 when biological productivity is high, POC/^{234}Th is greater in small particles instead of large.

A second trend in the POC/^{234}Th data is that POC/^{234}Th is elevated in large particles in the nepheloid layer (>4,000 m), but in the upper 200 m, it is greatest in small particles, with intermediate values in the

intervening water depths (Figs. S1, S2). This likely reflects the processes underlying the biological pump, whereby the largest organic particles aggregate and sink deep into the water column, and smaller organic particles lose their carbon content to remineralization before reaching great depths. Thus POC in the nepheloid layer is more strongly associated with larger particles, relative to particles found at lesser depths. An alternative explanation is that the large particles spend a finite length of time at the sediment-water interface before resuspension and the ^{234}Th activity in them has decayed.

Total seawater ^{234}Th

The ^{234}Th in total seawater, (primarily dissolved, but also including a small component of particulate ^{234}Th) was measured in the upper 300 m on five cruises (Fig. S3; **Error! Reference source not found.**Dataset S1). ^{234}Th activity was less than that of its parent isotope, ^{238}U, at most depths, indicating removal of ^{234}Th from the euphotic zone by scavenging. This deficit was typically greatest in the upper 100 m, where scavenging is most intense, and declined with depth. During some cruises, surpluses of ^{234}Th were found at depths greater than 100 m, indicating return of scavenged thorium to the water column by remineralization of particles. There was a seasonal component to the deficits as well, with strong surface deficits during May, June, and August, and lesser surface deficits in November and February.

The ^{234}Th deficits at individual depths were integrated trapezoidally to calculate the ^{234}Th deficit in the upper 100 m and 300 m of the water column (Table S3). Deficits integrated to 100 m are in the range of 300–800 Bq/m^2. Deficits integrated to 300 m are in the range of 400–2,700 Bq/m^2 and carry a greater degree of uncertainty due to the inclusion of depths in integration in which ^{234}Th in near secular equilibrium with ^{238}U. The integrated deficits multiplied by the 234Th decay constant (10.51 yr^{-1}) give the ^{234}Th removal flux (assuming no non-steady-state or circulation effects) (Fig. S3).

There was a strong component of seasonality to the deficits, with the greatest deficits (integrating to either depth) occurring during August, and the smallest deficits occurring in February. For the deficits to peak in late summer, when biological productivity has slowed, rather than in May or June, suggests that advective mixing is an important component of the ^{234}Th budget in the upper water column. Deficits are low when the water column is well-mixed in the cold months and higher when the water column is stratified. Alternatively, the higher late summer deficits may reflect the sinking of biogenic particles produced during the higher productivity of May-June.

Carbon Export

Export of particulate organic carbon to 100 m was calculated by multiplying the POC/^{234}Th measured on the large particle fraction filtered at 100 m by the integrated ^{234}Th deficit to that depth. Sufficient data was available to estimate POC flux on three cruises- May and August, 2012 and June, 2013. The flux was found to be lowest in May and higher in June and August (Table S4).

Table S1. Particulate ^{234}Th activities on a variety of filters collected at the Bermuda Rise Flux Experiment (BaRFlux) site (33°N, 55°W) in June 2013. Pumps were loaded with either (top to bottom) polyester/QM-A1/QM-A2 or polyester/Supor filters and on some casts were paired 20 m apart, e.g. 60 and 80 m, etc. to aid comparison.

Depth m	Cast date	Particulate ^{234}Th mBq/L 1–70 µm (QM-A1)	Particulate ^{234}Th mBq/L 1–70 µm (QM-A2)	Particulate ^{234}Th mBq/L 0.8–70 µm (Supor)	Particulate ^{234}Th mBq/L >70 µm (polyester)
60	Jun 7	-	-	1.288	0.090
80	Jun 7	2.757	0.410	-	0.318
90	Jun 3	-	-	1.169	0.330
110	Jun 3	2.322	0.205	-	0.597
140	Jun 7	-	-	2.380	0.487
160	Jun 7	1.360	0.227	-	0.115
290	Jun 3	-	-	1.520	0.127
310	Jun 3	1.042	0.131	-	0.119
500	Jun 5	-	-	0.769	0.092
1000	Jun 5	1.612	0.163	-	0.116
1000	Jun 4	-	-	1.123	0.083
1500	Jun 5	0.925	0.110	-	0.068
1500	Jun 4	-	-	0.831	0.089
2000	Jun 5	0.725	0.150	-	0.047
2000	Jun 4	-	-	0.857	0.131
2490	Jun 6	-	-	0.766	0.053
2990	Jun 6	-	-	0.635	0.048
3010	Jun 6	0.536	0.156	-	0.040
3500	Jun 4	-	-	0.454	0.054
3990	Jun 5	-	-	0.543	0.089
4010	Jun 5	0.675	0.158	-	0.065
4190	Jun 5	-	-	0.572	0.089

Table S2. Particulate ^{234}Th activities from the BaRFlux site in May 2012 in which daily variability in particulate concentrations was assessed by sampling the same depth on different days.

Cast date (2012)	Depth m	Particulate ^{234}Th mBq/L 1–70 µm (QM-A)	Particulate ^{234}Th mBq/L >70 µm (polyester)
May 8	100	2.553	0.545
May 13	100	1.229	0.325
May 12	300	1.341	0.161
May 13	300	1.277	0.065
May 8	1000	1.413	0.011
May 13	1000	2.164	0.067
May 9	1500	1.125	0.026
May 12	1500	1.402	0.062
May 9	2000	1.070	0.045
May 12	2000	1.257	0.034
May 10	3500	0.684	0.045
May 11	3500	0.719	0.028
May 10	4000	1.023	0.071
May 11	4000	1.079	0.055
May 10	4200	1.999	0.101
May 12	4200	1.495	0.093

Table S3. Integrated deficits of total ^{234}Th activity calculated for the upper 300 and 100 m of the water column at the BaRFlux site.

Date	Deficit in 300 m		Deficit in 100 m	
	Bq/m^2	±	Bq/m^2	±
Feb 15, 2012	415	378	333	119
May 8-13, 2012	705	370	390	95
Aug 18-21, 2012	2683	310	813	95
Nov 16, 2012	2433	318	602	112
Jun 3-7, 2013	1750	338	795	107

Table S4. Particulate organic carbon flux at 100 m, derived from the ^{234}Th deficits in the upper 100 m and the POC/^{234}Th ratio found in >70 µm particles filtered at 100 m (Dataset S1) for the BaRFlux site. (Interpolation was used to calculate the POC/^{234}Th ratio at 100 m in August, 2012 and June, 2013.)

Date	^{234}Th flux		POC/^{234}Th (1–70 µm)		POC/^{234}Th (>70 µm)		POC flux @ 100 m (1–70 µm)		POC flux @ 100 m (>70 µm)	
	Bq/m^2/yr	±	µmol/Bq	±	µmol/Bq	±	mmol/m^2/d	±	mmol/m^2/d	±
May 8-13, 2012	4105	993	473	24	172	48	5.3	2.0	1.9	0.7
Aug 18-21, 2012	8523	998	-	-	140	39	-	-	3.3	1.0
Jun 3-7, 2013	8351	1119	186	9	140	40	4.2	0.6	3.2	1.0

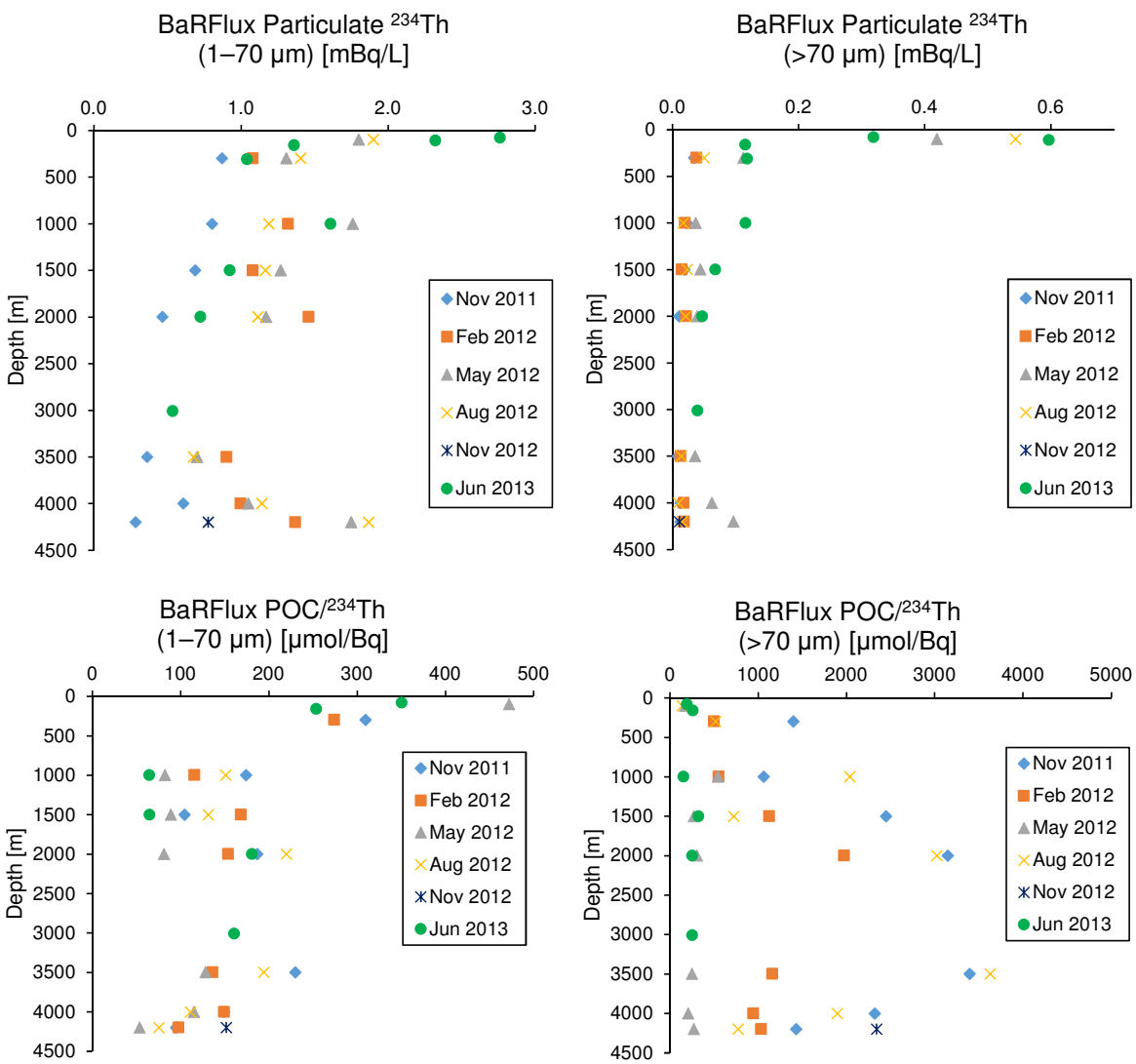

Figure S1. (Upper) Particulate ^{234}Th activity measured on filterable particles in the small size fraction (left), and large size fraction (right). (Lower) POC/^{234}Th ratios of small (left) and large (right) particles at the same BaRFlux time-series occupations.

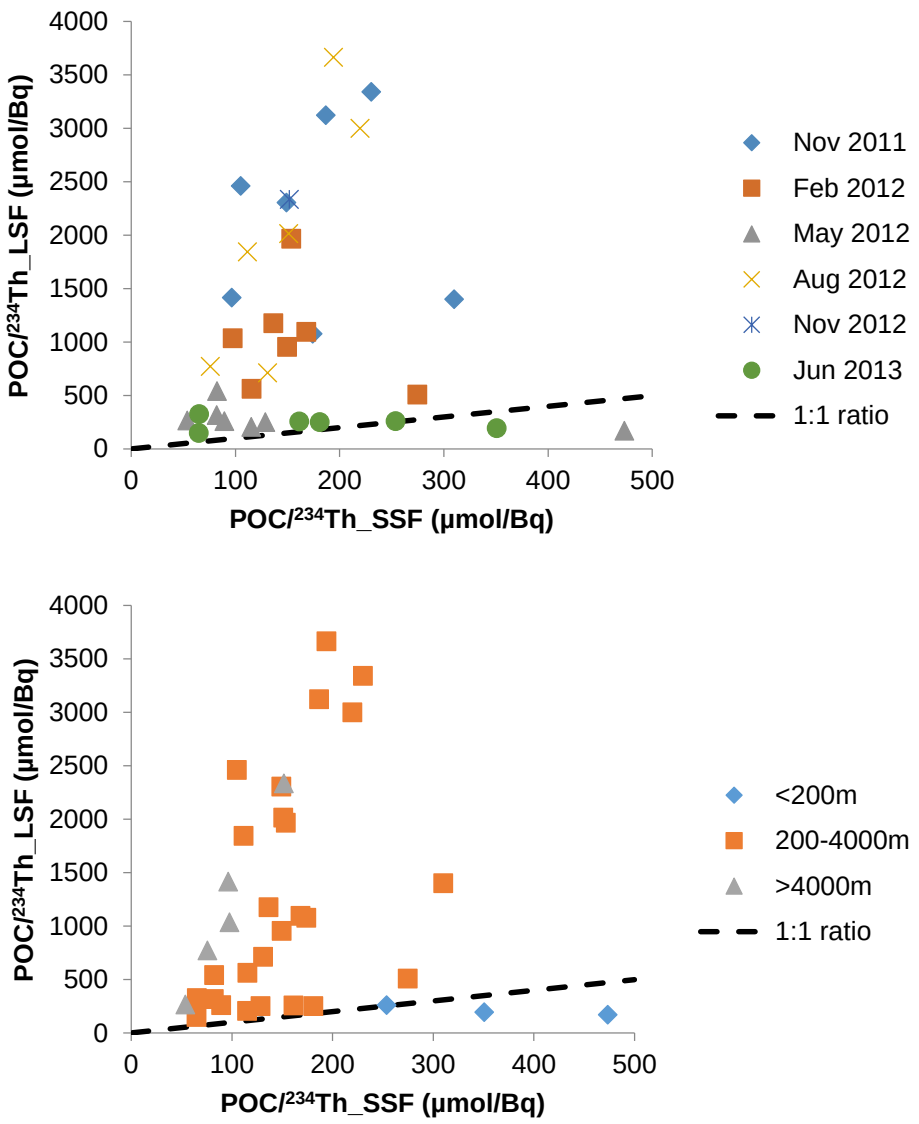

Figure S2. Comparison of POC/^{234}Th ratios in the smaller and larger size fractions from the BaRFlux site. The same data are displayed in two forms, separated by date (upper) and depth in the water column (lower).

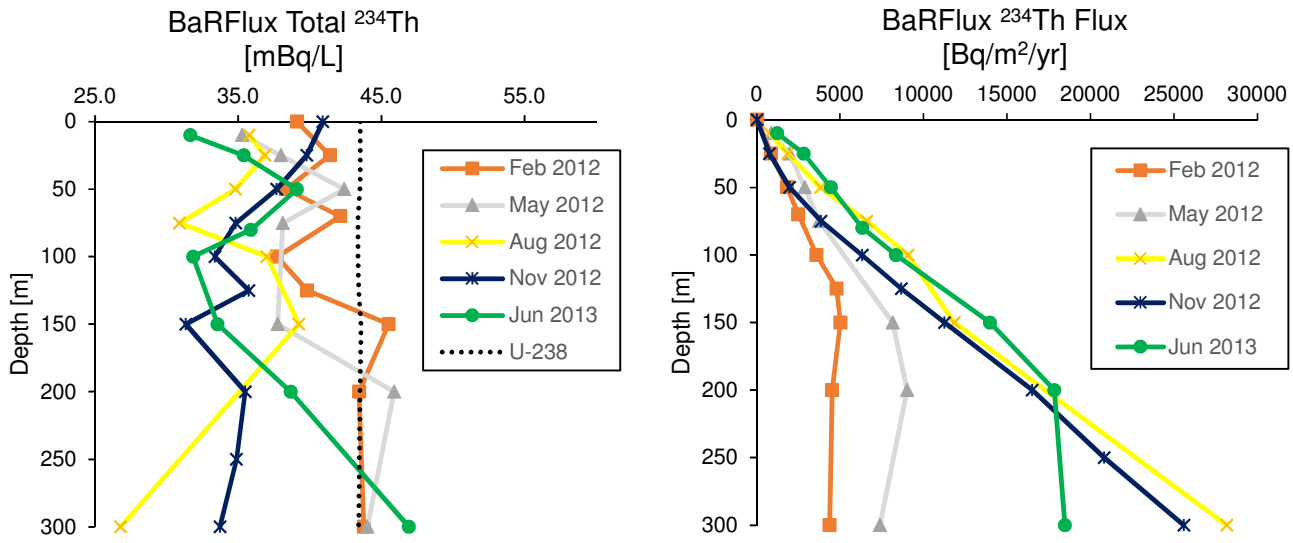

Figure S3. Total ^{234}Th activities, measured on unfiltered water, from the time-series occupations of the BaRFlux site (left). The dotted line is the ^{238}U activities in seawater, based on salinity (a typical profile is shown but for disequilibrium calculations, a ^{238}U profile was calculated for each cast that the ^{234}Th samples were taken from. (Right) Calculated ^{234}Th fluxes, based on integrated ^{234}Th : ^{238}U disequilibria, for the time-series occupations of the BarFlux site. Secular equilibrium was usually reached at this site around 150-200m, but in some cases extended throughout the entire measured water column of 300 m. For POC flux calculations, only the flux integrated to 100 m was used.

Supplemental Text 2.

Here we provide several supplemental plots for which space did not allow in the main text. First we show the comparison of ^{228}Th measured in the small size fraction (SSF, 1–51 μm) and large size fraction (LSF, >51μm) of particles collected by in situ pumps, but for which multiple LSF samples had to be combined to meet analytical requirements. Next we show plots of the derived fluxes from the 4 radionuclide pairs at the six additional sites (see Fig. 1 in the main text) whose results were not shown in the main text. Where possible, we compare flux results to other flux studies from the same or proximal locations and these studies are referenced in the figure captions.

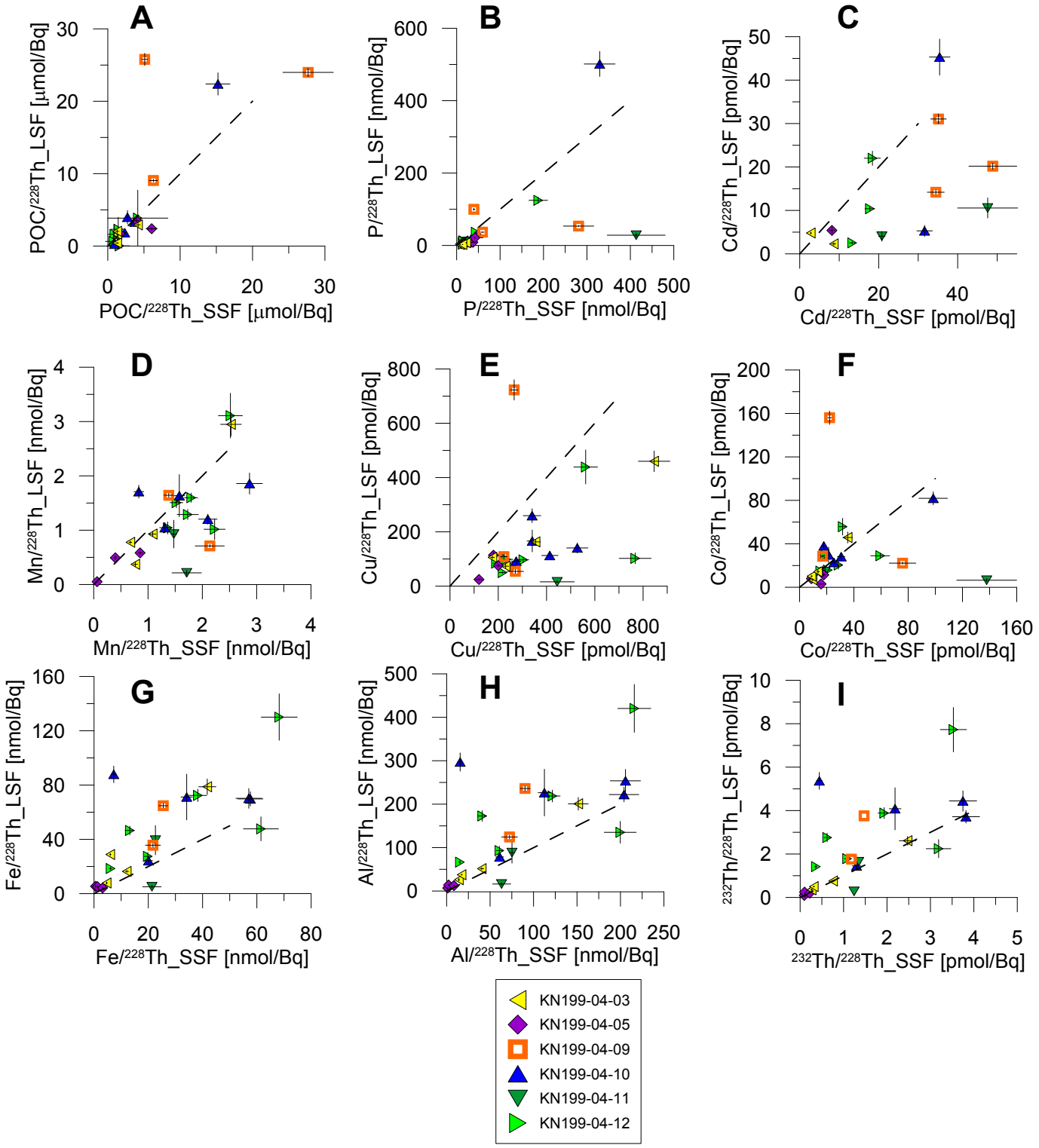

Figure S4. Cross plots of element to ^{228}Th ratios in large size fraction (LSF, >51 µm) of particles against the small size fraction (1-51 µm) of particles from select stations in GA03 (see Figure 1). The large particle ^{228}Th samples had to combine 2 or 3 samples, adjacent in depth, for analysis. Therefore the data are cross-plotted against averages of the elemental particle data for better comparison.

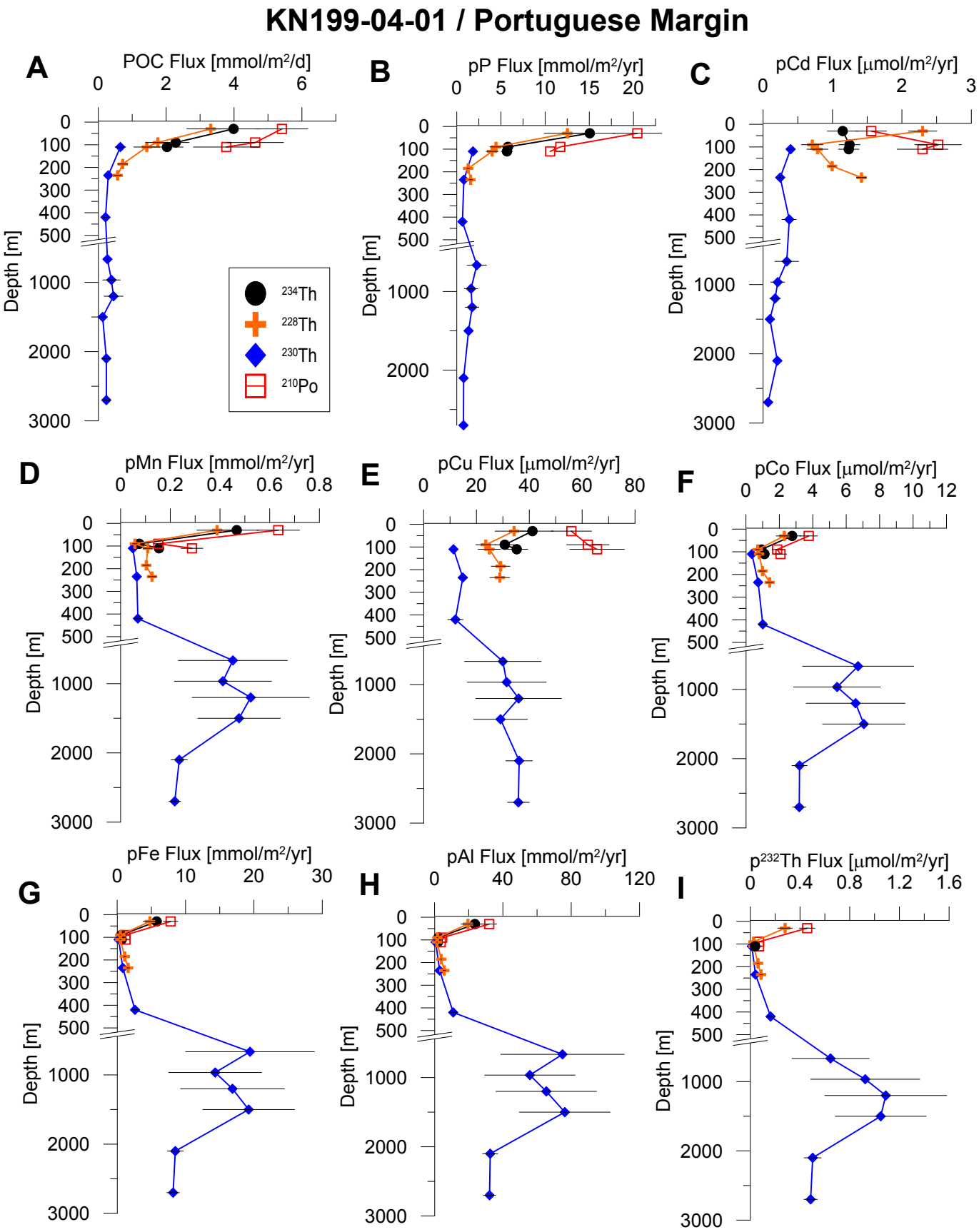

Figure S5. Particulate elemental fluxes derived for station KN199-04-01 from 4 radionuclide pairs. Where error bars (1SD) are not visible, they are smaller than the symbol size. The high fluxes within 500–1500 m depth reflect the admixture of particle-laden Mediterranean outflow water (Hayes et al., 2015).

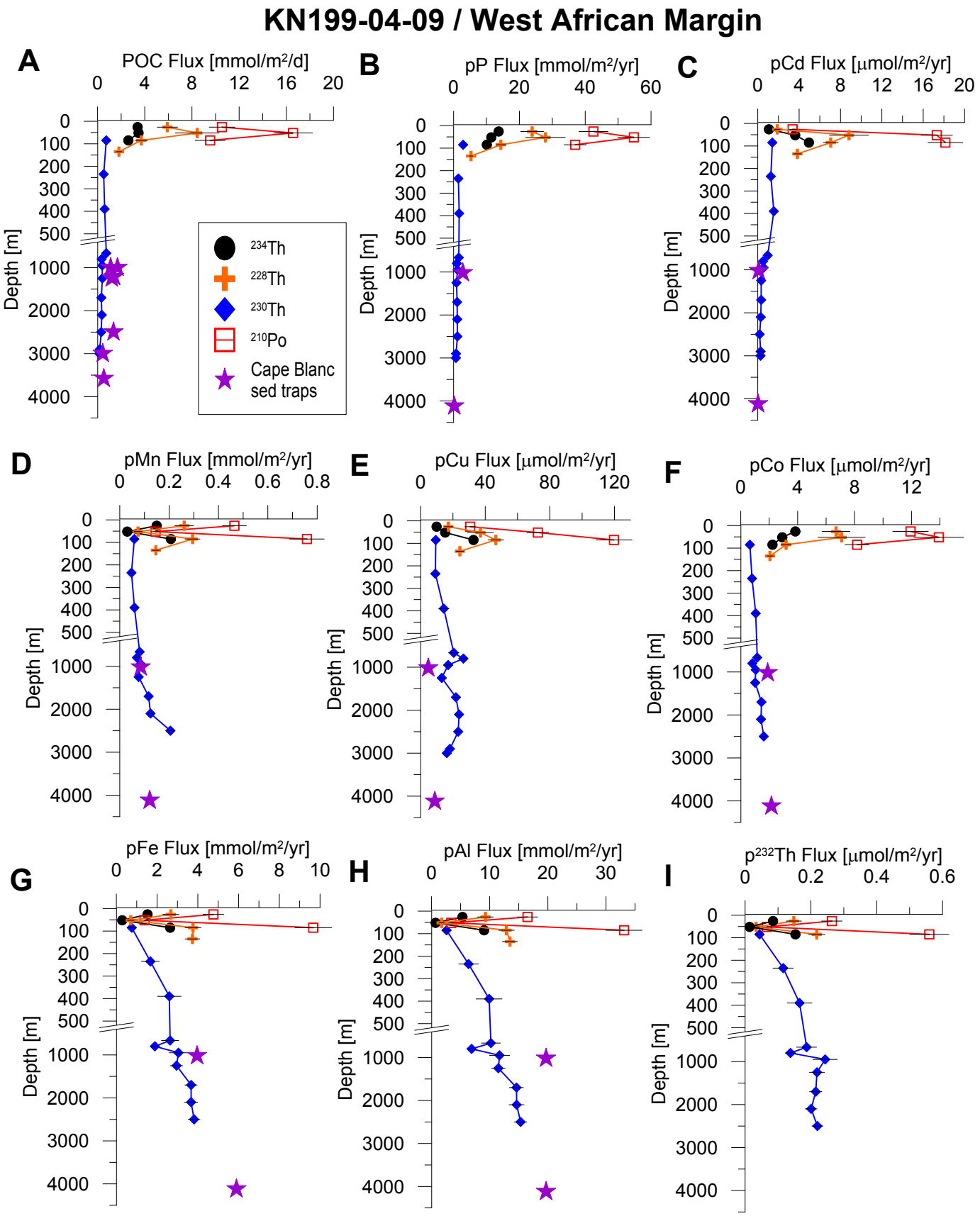

Figure S6. Particulate elemental fluxes derived for station KN199-04-09. In (B-H), the purple stars are sediment trap fluxes from a site offshore of Cape Blanc (Kremling and Streu, 1993). In (A), the purple stars are compiled deep POC fluxes from a series of sediment traps from the Cape Blanc area (Bory et al., 2001; Helmke et al., 2005; Nowald et al., 2015). A benthic nepheloid layer was observed at this station (Hayes et al., 2015; Lam et al., 2015) and therefore ^{230}Th-based fluxes are not shown below 2.5 km.

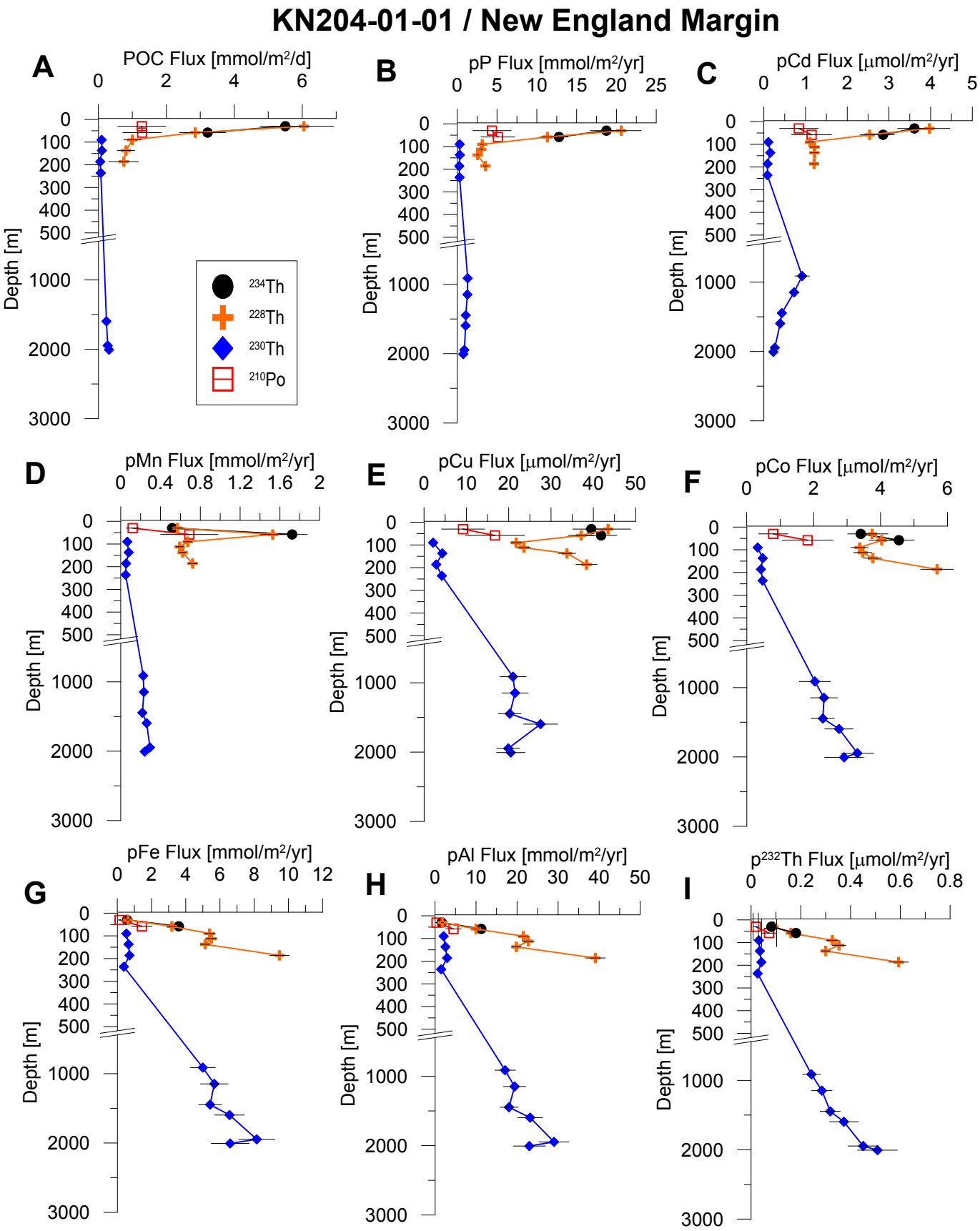

Figure S7. Particulate elemental fluxes derived for station KN204-01-01 from 4 radionuclide pairs. Where error bars (1SD) are not visible, they are smaller than the symbol size.

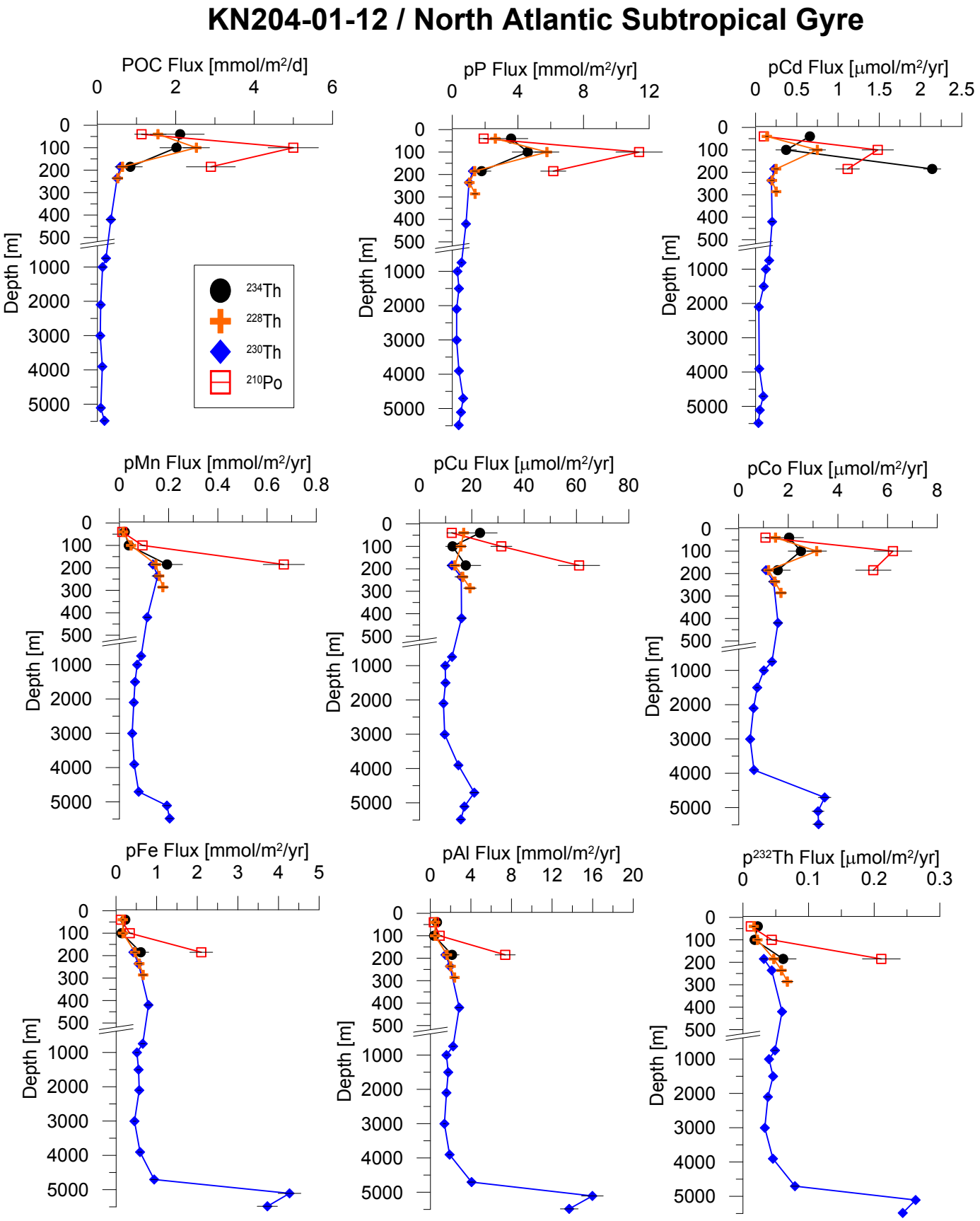

Figure S8. Particulate elemental fluxes derived for station KN204-01-12 from 4 radionuclide pairs. Where error bars (1SD) are not visible, they are smaller than the symbol size.

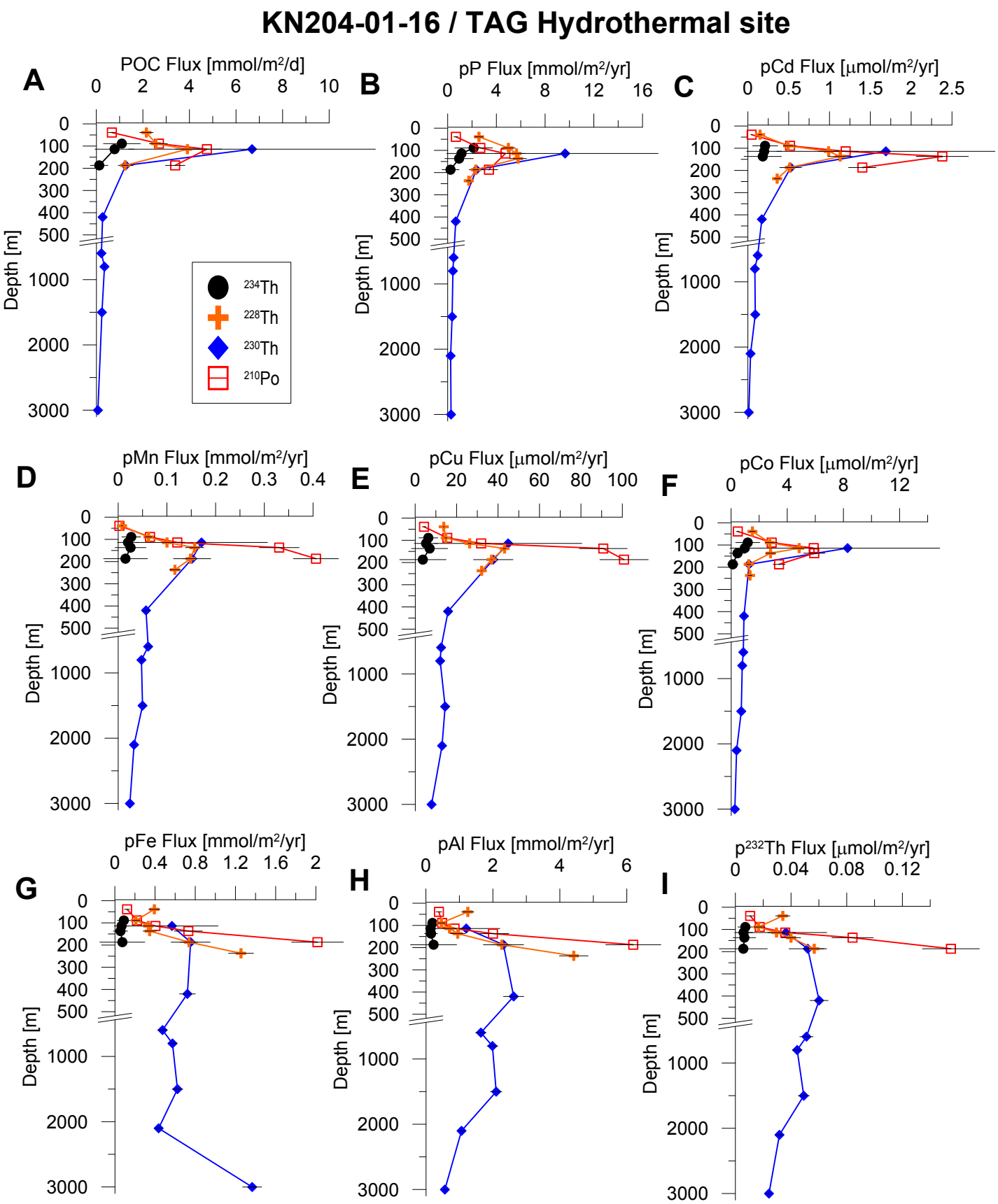

Figure S9. Particulate elemental fluxes derived for station KN204-01-16 from 4 radionuclide pairs. Where error bars (1SD) are not visible, they are smaller than the symbol size. Fluxes based on ^{230}Th-based fluxes below 3 km are influenced by a hydrothermal plume and therefore are not shown.

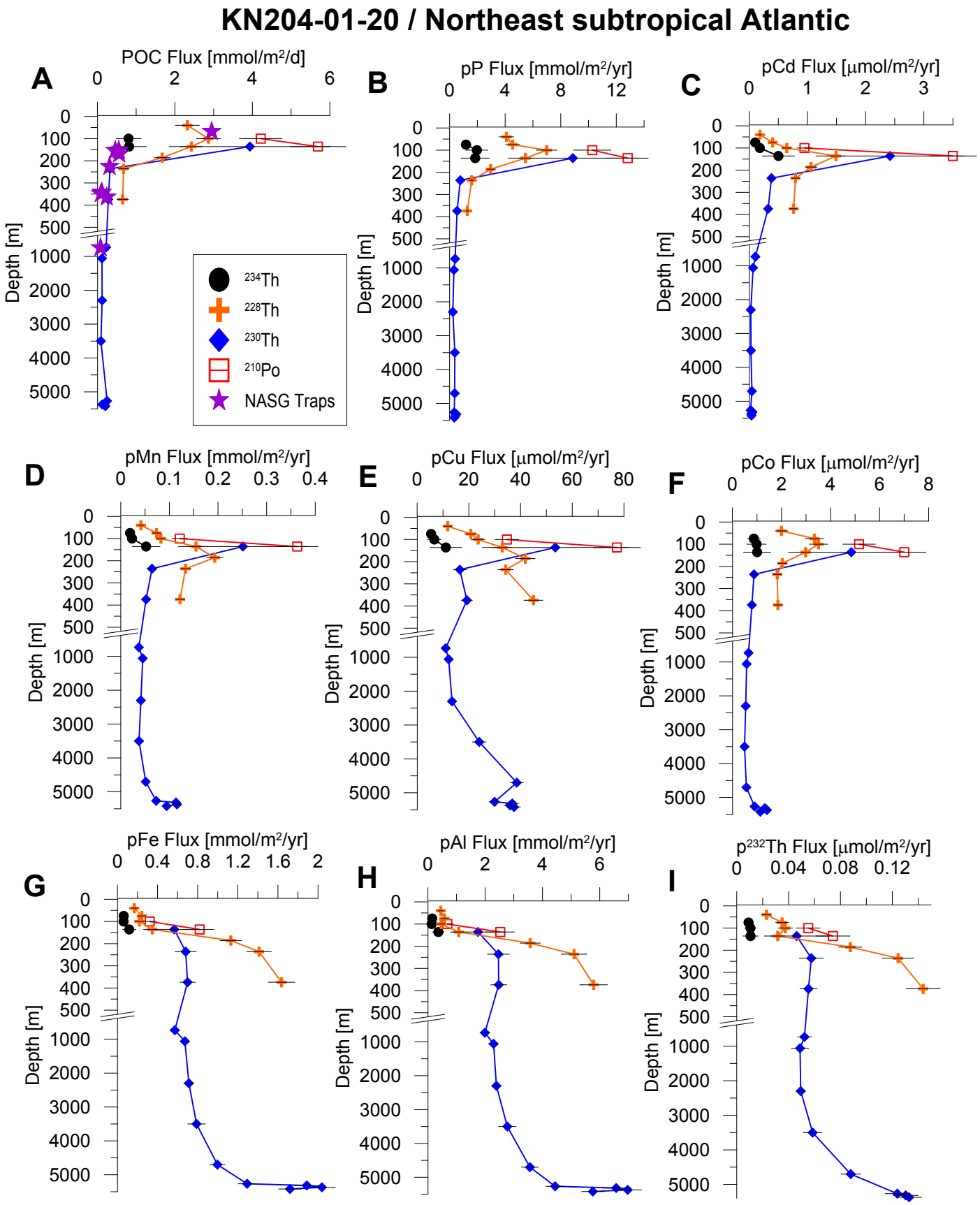

Figure S10. Particulate elemental fluxes derived for station KN204-01-20 from 4 radionuclide pairs. Where error bars (1SD) are not visible, they are smaller than the symbol size. (A) includes comparison to POC flux derived from neutrally buoyant sediment traps (Marsay et al., 2015) deployed at a site in the North Atlantic Subtropical Gyre (NASG; 26.5°N, 31.5°W) proximal to KN204-01-20 (22.3°N, 35.9°W).

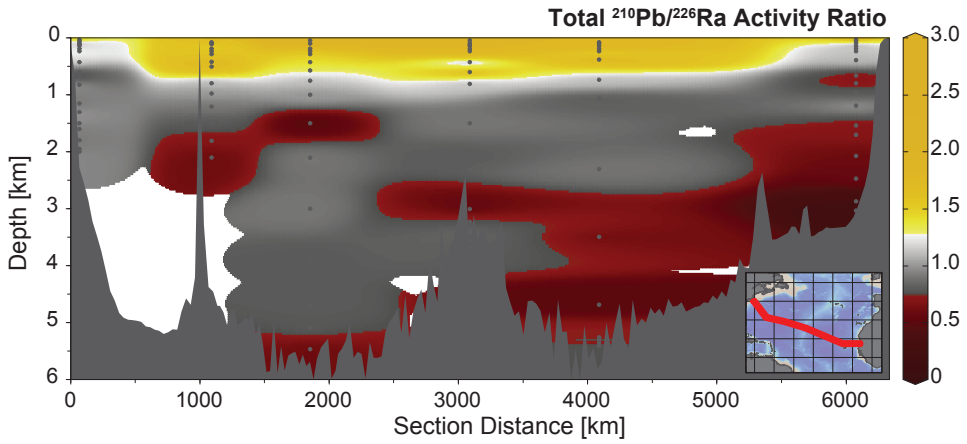

Figure S11. The activity ratio of ^{210}Pb over its grand-parent ^{226}Ra in the total (dissolved + particulate) phase for the GA03 transect (section corresponding to inset map) (Rigaud et al., 2015). The color scale is designed so that near secular equilibrium between the two isotopes is in gray, excess of the daughter is in yellow and a deficit of the daughter with respect to the parent is in red.

REFERENCES

Abramson, L., Lee, C., Liu, Z., Wakeham, S.G., Szlosek, J., 2010. Exchange between suspended and sinking particles in the northwest Mediterranean as inferred from the organic composition of in situ pump and sediment trap samples. Limnol. Oceanogr. 55, 725–739. https://doi.org/10.4319/lo.2009.55.2.0725

Auro, M.E., Robinson, L.F., Burke, A., Bradtmiller, L.I., Fleisher, M.Q., Anderson, R.F., 2012. Improvements to 232-thorium, 230-thorium, and 231-protactinium analysis in seawater arising from GEOTRACES intercalibration. Limnol. Oceanogr. Methods 10, 464–474. https://doi.org/10.4319/lom.2012.10.464

Bory, A., Jeandel, C., Leblond, N., Vangriesheim, A., Khripounoff, A., Beaufort, L., Rabouille, C., Nicolas, E., Tachikawa, K., Etcheber, H., Buat-Ménard, P., 2001. Downward particle fluxes within different productivity regimes off the Mauritanian upwelling zone (EUMELI program). Deep Sea Res. I 48, 2251–2282. https://doi.org/10.1016/S0967-0637(01)00010-3

Buesseler, K.O., Benitez-Nelson, C., Rutgers van der Loeff, M., Andrews, J., Ball, L., Crossin, G., Charette, M.A., 2001. An intercomparison of small- and large-volume techniques for thorium-234 in seawater. Mar. Chem. 74, 15–28. https://doi.org/10.1016/S0304-4203(00)00092-X

Cochran, J.K., Masqué, P., 2003. Short-lived U/Th Series Radionuclides in the Ocean: Tracers for Scavenging Rates, Export Fluxes and Particle Dynamics. Rev. Mineral. Geochemistry 52, 461–492. https://doi.org/10.2113/0520461

Hayes, C.T., Anderson, R.F., Fleisher, M.Q., Huang, K.F., Robinson, L.F., Lu, Y., Cheng, H., Edwards, R.L., Moran, S.B., 2015. ^{230}Th and ^{231}Pa on GEOTRACES GA03, the U.S. GEOTRACES North Atlantic transect, and implications for modern and paleoceanographic chemical fluxes. Deep Sea Res. II 116, 29–41. https://doi.org/10.1016/j.dsr2.2014.07.007

Helmke, P., Romero, O., Fischer, G., 2005. Northwest African upwelling and its effect on offshore organic carbon export to the deep sea. Global Biogeochem. Cycles 19, 1–16. https://doi.org/10.1029/2004GB002265

Kremling, K., Streu, P., 1993. Saharan dust influenced trace element fluxes in deep North Atlantic subtropical waters. Deep Sea Res. I 40, 1155–1168. https://doi.org/10.1016/0967-0637(93)90131-L

Lam, P.J., Ohnemus, D.C., Auro, M.E., 2015. Size-fractionated major particle composition and concentrations from the US GEOTRACES North Atlantic Zonal Transect. Deep Sea Res. II 116, 303–320. https://doi.org/10.1016/j.dsr2.2014.11.020

Marsay, C.M., Sanders, R.J., Henson, S.A., Pabortsava, K., Achterberg, E.P., Lampitt, R.S., 2015. Attenuation of sinking particulate organic carbon flux through the mesopelagic ocean. Proc. Natl. Acad. Sci. U. S. A. 112, 1089–94. https://doi.org/10.1073/pnas.1415311112

Nowald, N., Iversen, M.H., Fischer, G., Ratmeyer, V., Wefer, G., 2015. Time series of in-situ particle properties and sediment trap fluxes in the coastal upwelling filament off Cape Blanc, Mauritania. Prog. Oceanogr. 137, 1–11. https://doi.org/10.1016/j.pocean.2014.12.015

Pates, J.M., Muir, G.K.P., 2007. U–salinity relationships in the Mediterranean: Implications for Th:^{238}U particle flux studies. Mar. Chem. 106, 530–545. https://doi.org/10.1016/j.marchem.2007.05.006

Rigaud, S., Stewart, G., Baskaran, M., Marsan, D., Church, T., 2015. ^{210}Po and ^{210}Pb distribution, dissolved-particulate exchange rates, and particulate export along the North Atlantic US GEOTRACES GA03 section. Deep Sea Res. II 116, 60–78. https://doi.org/10.1016/j.dsr2.2014.11.003